Cao, C., Hill, T., & Conn, A. (2019). On the nonlinear dynamics of a circular dielectric elastomer oscillator. *Smart Materials and Structures*, *28*(7), [075020]. https://doi.org/10.1088/1361-665X/ab1cc8

On the nonlinear dynamics of a circular dielectric elastomer oscillator

On the nonlinear dynamics of a circular dielectric elastomer oscillator

Chongjing Cao[1, 2], Thomas L. Hill,[3] and Andrew T. Conn[1,3]

[1.] Bristol Robotics Laboratory, Bristol, BS16 1QY, UK

[2.] Department of Aerospace Engineering, University of Bristol, BS8 1TR, Bristol, UK

[3.] Department of Mechanical Engineering, University of Bristol, BS8 1TR, Bristol, UK

Email addresses: C. Cao (cc15716@bristol.ac.uk), T. Hill (tom.hill@bristol.ac.uk), A. Conn (a.conn@bristol.ac.uk).

Abstract

Dielectric elastomer actuators (DEAs) are an emerging soft actuation technology that have advantages in large actuation strain, inherent compliance and low cost. Resonant actuation of DEAs has been shown to increase the actuation stroke and power output and has been utilized in applications such as robotic locomotion and loudspeakers. In this work, we present a planar circular dielectric elastomer oscillator (DEO) that can exert out-of-plane deformation as large as 80 % of its own diameter at resonance. By experiments and model simulation we show that this simple DEO design exhibits complex nonlinear responses, including multiple solutions, sub- and super-harmonics, and exhibits multiple resonant peaks. The DEO performance is characterized against membrane pre-stretch and the weight of the attached mass and its actuation signals (DC and AC amplitudes). The resonant frequency and the amplitude are found to be easily tuned by varying these parameters. Such large stroke output and highly tunable resonance make this DEO a promising candidate for applications such as active vibration absorption, embedded loudspeakers, soft pumps and robotic locomotion.

Key words: dielectric elastomer oscillator, nonlinear dynamics, custom carbon grease, out-of-plane deformation

1. Introduction

Dielectric elastomer actuators (DEAs) are an emerging soft actuation technology that show advantages over conventional actuators in terms of large actuation strain, inherent compliance and low

cost [1]. An ideal DEA consists of a piece of elastomer membrane sandwiched between two compliant electrodes. When a voltage is applied across the electrodes, the electric field generates Maxwell stress that causes the elastomer to contract in thickness and expand in area. Due to the inherent elasticity of the actuator, when stimulated by an alternating voltage at a frequency close to one of its natural frequencies, the DEA can exhibit a significant increase in its actuation strain. The dynamic behaviors of hyperelastic materials have been studied in the past (see e.g. [2] [3] [4]) and several works have investigated the dynamics of dielectric elastomers. For example, pneumatically-coupled DEAs [5] [6] [7] [8] have been previously investigated via either analytical models or experiments and have demonstrated subharmonic, harmonic and super-harmonic responses. In previous works [9] [10], the resonance phenomena of double cone DEAs and its application to flapping wing micro air vehicles have been demonstrated. In this work, we focus on a planar circular DE oscillator (DEO) configuration (after [1] [11] [12] [13] [14] [15]) that exhibits out-of-plane deformation at resonance and it has advantages over other aforementioned DEO designs in terms of ease of fabrication and simplicity of structure (i.e. low-profile two-dimensional structure without biasing elements such as pressure or spring). In [11], a stretchable and transparent DEO loudspeaker was demonstrated with the capability of operating at frequencies over 10 kHz. In [14], a vibrational robot with a DEO as the excitation source was developed and different resonant modes were utilized for steering. In the previous work [16], we have integrated a DEO with an integrated electroadhesion gripper and by using the out-of-plane vibration at its resonance, the release process of this electroadhesion gripper was sped up by over 100 times.

Despite these promising applications of DEOs, previous works have focused solely on analyzing the out-of-plane deformation amplitudes at its resonance and the shapes of each resonant mode, while the complex frequency-dependent response has not been investigated. The strong nonlinearity of the DEO suggests a complex frequency response and demands further in-depth studies using both experimental approach and mathematical modelling. The effects of pre-stretch ratios and actuation electric field, which have been shown to have significant effects on the performance of a DEA [17] [18], have not been investigated on this DEO configuration in the past. These factors demand that a comprehensive study of this DEO configuration's frequency response is required to better understand how it can be fully exploited in applications such as active vibration damping and robotic locomotion.

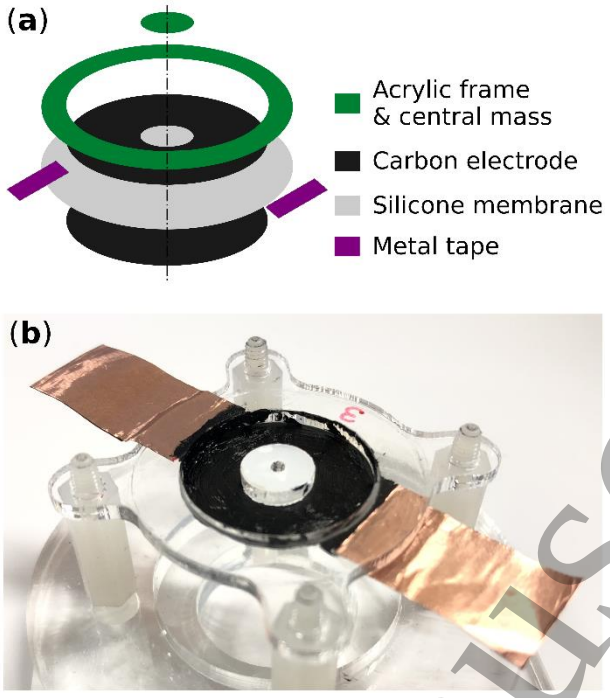

Figure 1. (**a**) Exposed assembly view of the dielectric elastomer oscillator. (**b**) Photo of the fabricated prototype.

In this work, we report a DEO design which exhibits complex nonlinear resonance with hysteresis and under different excitation frequencies, the DEO demonstrates different frequency responses (sub- and super- harmonic resonances are observed). A schematic diagram and a fabricated prototype of the DEO are shown in **Figure 1**. Carbon electrodes, commonly in the form of carbon grease, have been used as the compliant electrodes of DEAs. However, one critical issue of commercially available carbon greases, which use silicone oil or other synthesis oils as the solvents, is that they are not compatible with the silicone elastomer (Elastosil, Wacker Chemie AG) commonly adopted in DEA researches (see e.g. [9] [19] [20] [21] [22]), as was found in [23]. This could be due to the fact that silicone oil can be absorbed by the silicone elastomer, which causes the swelling of the elastomer and thus significantly affects its mechanical and electrical properties. As a result, before any dynamic analysis on the DEO is conducted in this work, it is essential to develop a custom carbon grease as the compliant electrodes to eliminate the swelling effect on the silicone membrane.

The structure of this paper is described as follows. In Section 2, a custom carbon grease is developed. The fabrication process of the custom carbon grease is reported, and its electrical conductivity and mechanical properties are compared with the commercially available counterpart. In Section 3, a mathematical model is developed to characterize both the quasi-static and dynamic response of the DEO. In Section 4, the setups for the quasi-static and dynamic experiments are described. In Section 5, by both experiment and numerical simulation, we analyze the extremely complex nonlinear frequency response of the DEO. In Section 6, the effects of pre-stretch of the DE membrane and actuation electric

field on the dynamic performance of this oscillator are investigated. In previous work [16], we found that by adding an additional mass to the centre of the membrane, the oscillation amplitude can be improved. Hence in this section, we also analyze the effect of the mass added to the membrane on the resonance of the DEO. Finally, in Section 7, conclusions are drawn and future work is discussed.

2. Development of custom electrode

As an essential part of any DEA, idealised compliant electrodes shall have good conductivity across a large range of strains and have minimum impact on the stiffness of the dielectric elastomer. The most common compliant electrodes for DEAs are carbon-based, which include loose carbon powder; carbon grease (carbon particles mixed in a viscous oil) and carbon/elastomer compound (carbon particles mixed into a crosslinked elastomer) [24]. Loose carbon powder tends to have significant larger resistance at large strains (> 100 %) [25] [26] than carbon grease and carbon/elastomer compound, thus it was not investigated in this work. Commercially available carbon grease (such as MG 846, MG Chemicals, used in this study) has the problem of diffusion into silicone elastomers [23] [24], which can cause swelling of the elastomer, thus affecting the performance of the DEA. This is believed to be due to the silicone oil solvent being absorbed by the silicone membrane. Hence in this work, we first develop a custom carbon grease which does not cause swelling of the silicone elastomer. This section reports the fabrication process of this custom carbon grease and the comparison between it and commercially available carbon grease MG 846 and a carbon/elastomer compound.

2.1 Fabrication of the electrodes and DEOs

In [23], castor oil and carbon black powder have been mixed to make silicone-oil-free carbon grease and it was found to be compatible with Elastosil silicone films, as used in this study. Following their work, we adopt a vegetable oil solvent which is also compatible with Elastosil silicone films but has a much lower viscosity (< 0.06 Pa·s at 26 ˚C [27]) with added benefits of low-cost and high commercial availability. Three custom carbon greases, with different carbon black to vegetable oil weight ratios of 10 %, 15 % and 20 %, were fabricated. The fabrication process is described as follows. First, 10/15/20 wt.% carbon black powders (1333-86-4, Cabot Corporation, USA) and 90/85/80 wt.% vegetable (rapeseed) oil (ASDA, UK) were added to a mixing cup. The mixture was first stirred by a mixer (Model 50006-13, Cole-Parmer, UK) at the speed of 100 rpm for 1 min and then 600 rpm for 5 mins to achieve a homogenous dispersion. Carbon-vegetable-oil mix with carbon powder greater than 20 wt.% was found to be too viscous to be mixed by the mixer, hence a 20 wt.% carbon powder was set as the upper

limit for this custom carbon grease. Fabricated carbon grease, as well as commercial carbon grease, MG 846, were applied to the silicone elastomer by a hand brush.

A carbon/elastomer compound electrode was fabricated by mixing 10 wt.% carbon powder and 90 wt.% uncured silicone (Ecoflex 20, Smooth-on, USA) using the same method and applied on the dielectric elastomer using a mask and scraper and left to cure for 24 hours at room temperature (20 ˚C) (following [28] [29]).

To fabricate the DEO, an off-the-shelf silicone elastomer (Elastosil, thickness 50 μm, Wacker Chemie AG) was used as the membrane. Except where noted in Section 6.1, for all test, the membrane was pre-stretched biaxially by λ_p = 1.2 × 1.2, where λ_p is the pre-stretch ratio, and then bonded to an acrylic ring (20 mm inner diameter) using silicone adhesive (Sil-poxy, Smooth-On). An acrylic disk (0.1 g, 8 mm outer diameter) was bonded to the centre of the membrane using the same method. Copper tapes were used as the connection between the carbon electrodes and high voltage cables.

2.2 Effect of electrode type on the mechanical response of DEOs

First, the effects of different complaint electrodes on the mechanical properties of the silicone membrane was investigated. The experiment is described as follows. The fabricated DEO samples were fixed to the testing rig, a linear rail (X-LSQ150B-E01, ZABER) deforms the centre of the DEO membrane out-of-plane from 0 to 6 mm at a low velocity of 0.05 mm/s and a load cell (NO.1004, TEDEA) was used to measure the reaction force of the DEO. Detailed experimental setup can be found in Section 4.

In **Figure 2** (**a**), the quasi-static force-displacement curves of the DEOs with different electrodes are shown. The custom carbon grease only caused a negligible increase in the net stiffness, while both commercial carbon grease MG 846 and the carbon/elastomer compound caused significant softening effect on the membrane at small displacements. As the displacement increases, the added stiffness from the carbon/elastomer electrode clearly increased of the overall stiffness of the DEO. It can also be noted that, for these three electrodes, custom carbon grease shows the smallest hysteresis, which suggests a lower viscosity during dynamic actuation. Apart from the effect on the stiffness of the elastomer, the swelling effect can be more visible on the physical appearance. **Figure 2** (**b**) compares the DEOs with the three different electrodes applied. No pre-stretch was applied to the silicone membranes to demonstrate the swelling effect more clearly. One can see that the membrane with custom carbon grease shows no wrinkle and the membrane remained flat. However, for commercial carbon grease and carbon/elastomer electrodes, wrinkles can be cleared observed, and membranes buckled due to swelling

(note that his wrinkling mechanism is distinct from loss of tension due to Maxwell pressure, as described in [30]).

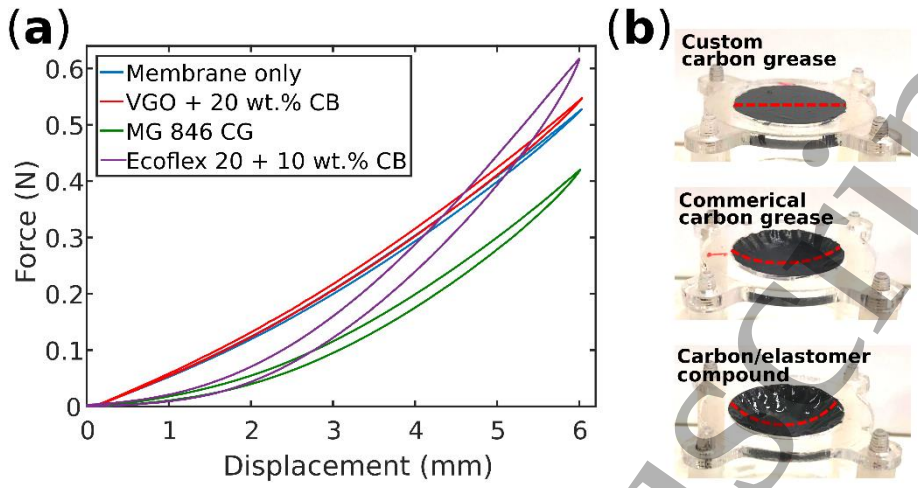

Figure 2. (**a**) Force-displacement curves of the DEO samples with no electrode (blue), vegetable oil + 20 wt.% carbon black (red), carbon grease MG 846 (green), Ecoflex 20 + 10 wt.% carbon black (violet). Silicone elastomers were pre-stretched by λ_p = 1.2 × 1.2. (**b**) Comparison of the effects of the carbon-based electrodes on silicone elastomer. Top: custom carbon grease; middle: commercial carbon grease; bottom: carbon/elastomer compound. No pre-stretch for the membranes. Photos were taken 48 hours after the electrodes were applied. (CG = carbon grease, VGO = vegetable oil, CB = carbon black)

A second characteristic was investigated by measuring the damping of the electrodes. Since the carbon/elastomer compound causes the most severe swelling effect in **Figure 2**, in the following comparison, this electrode type is not included. To investigate the effect of carbon black concentration on the damping of DEOs, a step disturbance was applied to the DEO and the decaying displacement of the DEO as a function of time was recorded. The DEO samples were fixed to the testing rig, and the central mass of each DEO sample was stretched out-of-plane by 4 mm via a string and fixed. The string was then cut off to allow the mass together with the membrane oscillated freely. A laser displacement sensor was used to measure the decaying displacement after the step disturbance. Detailed time-displacement results are plotted in **Figure 3**. For DEO samples with 10, 15 and 20 wt.% carbon greases, the decaying time constants (the time it takes for the amplitude to decay to 36.8 % of its initial value) are 0.12 s, 0.135 s and 0.138 s respectively. As a comparison, the time for DEOs with MG 846 was 0.09 s. This result suggests that despite the increase in carbon black concentration and the more viscous feel during fabrication, 20 wt.% carbon grease does not cause an increase in the damping coefficient of the system and the damping effect of the custom carbon grease is lower than MG 846. Reduced damping will allow a greater resonant amplitude of the DEO, which can be advantageous in dynamic applications.

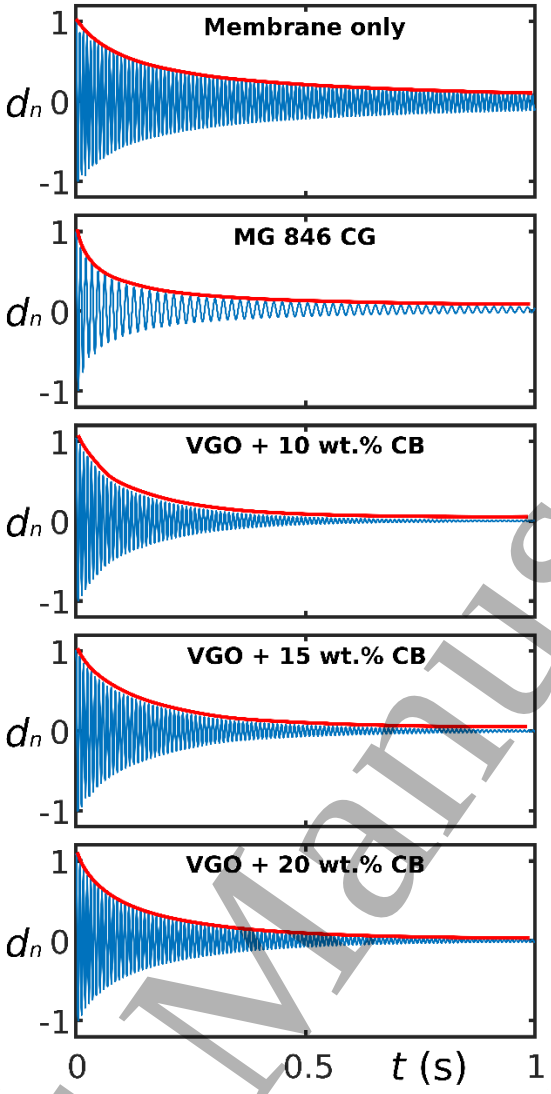

Figure 3. Passive step response of the DEOs with no electrode, MG 846, custom carbon grease with 10, 15 and 20 wt.% carbon black powder. d_n is the normalized displacement. (CG = carbon grease, VGO = vegetable oil, CB = carbon black)

2.3 Compliant electrode surface resistance measurements

In this test, the surface resistance of the custom carbon grease with different carbon concentrations and commercial carbon grease MG 846 are compared. Long and thin rectangular strips of carbon grease are hand brushed on a flat acrylic sheet and the length and width of these strips are 50 mm and 10 mm respectively (5:1 aspect ratio as recommended by [31]). Care has been taken to ensure an even electrode thickness. A high-precision LCR meter (E4980AL, Keysight) was utilized to measure the surface

resistance at 1,000 Hz. Copper tapes serve as the connection between the carbon grease and the LCR meter cables. Three samples were prepared for each concentration of carbon grease.

The experimental results are compared in **Figure 4** with detailed values listed in Table S1 in the supplementary material. As the concentration of the carbon black increases, the surface resistance reduces dramatically, resulting in a significantly improved conductivity. As the concentration reached 20 wt. %, which is the same as the MG 846, the custom carbon grease shows a lower surface resistance than MG 846 (2.1 kΩ/sq comparing to 3.2 kΩ/sq). This suggested that the custom carbon grease has an improved conductivity, which can reduce the RC time constant and improve the DEO's electrical response. By considering the conductivity and the low damping effect, custom carbon grease with 20 wt.% carbon particles was considered the best-performing overall and was adopted for the rest of studies.

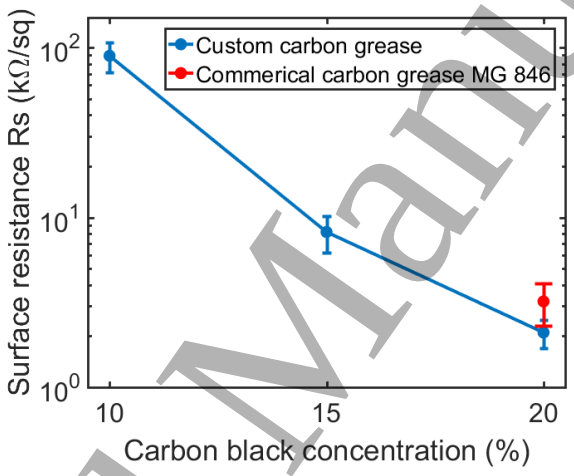

Figure 4. Measured surface resistance of the commercial carbon grease (20 wt.% carbon black powder), custom carbon grease with 10, 15 and 20 wt.% carbon black powder.

3. DEO numerical model

This section presents a numerical model that describes the dynamic response of the DEO at varying excitation frequencies. Note that in this DEO design, the exposed membrane is completely covered by compliant electrode, under the gravitational force, the in-plane expansion of the membrane when actuated is converted into an out-of-plane deformation and transits into a conical shape. This model was adapted from a conical shape DEA model in [19] which includes the following simplifying assumptions: (**i**) this is a 1 degree-of-freedom system, i.e. central mass only translates along the vertical axis; (**ii**) the deformed DEO is a truncated cone shape; (**iii**) the film thickness does not vary radially or circumferentially in a specific deformed position; (**iv**) the circumferential deformation of the membrane

is constant throughout the actuation. In [19], a linear spring-dashpot model was used to describe the viscoelasticity of the elastomer, while in this work this linear model is substituted by a hyperelastic spring-dashpot model, which is able to describe the nonlinear membrane stiffness more accurately across a wider range of deformation. Here we also neglect the effects of electrical response of the DEO as the measured RC time constant is less than 10^{-4} s, which suggests that at frequencies less than 1,000 Hz, the electrical response time can be neglected.

This model is illustrated in **Figure 5**. At the reference state, the dielectric elastomer does not experience any stretch, λ, and has an initial thickness T_0. The membrane is then stretched biaxially by $\lambda_p \times \lambda_p$ and bonded to a rigid circular frame with the inner radius, b, and a central disk with the radius, a. Assuming the membrane has a constant volume (i.e. the principle stretches $\lambda_1\lambda_2\lambda_3 = 1$), the current thickness is $T_1 = T_0/\lambda_p^2$. The radial stretch is $\lambda_1 = \lambda_p$ and the circumferential stretch is $\lambda_2 = \lambda_p$. As the membrane undergoes an out-of-plane deformation, d, the membrane is stretched further radially and shifted from its original position by an angle, α. The new radial stretch can be defined as:

$$\lambda_1 = \frac{\sqrt{d^2+(b-a)^2}}{(b-a)}\lambda_p \,, \qquad \text{Equation (1)}$$

and based on assumption (**iv**), the circumferential stretch, $\lambda_2 = \lambda_p$, remains unchanged during out-of-plane deformation.

The current membrane thickness can be written as

$$T_2 = \frac{T_0}{\lambda_1\lambda_2}. \qquad \text{Equation (2)}$$

The angle between the membrane and the horizontal plane, α, can be expressed as

$$\sin\alpha = \frac{d}{\sqrt{d^2+(b-a)^2}}. \qquad \text{Equation (3)}$$

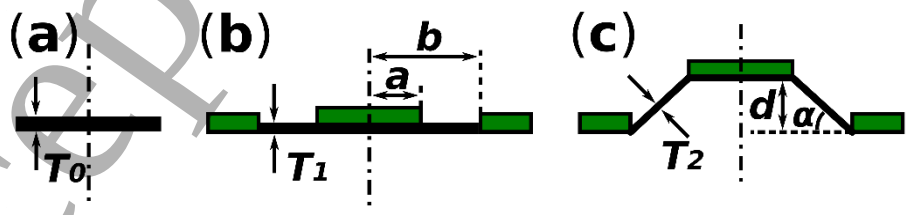

Figure 5. Schematic diagram of the DEO geometry. (**a**) A piece of circular silicone elastomer in its initial state. (**b**) Silicone membrane being stretched biaxially and then bonded to rigid frames. (**c**) When the centre is deformed out-of-plane, the DEO forms a conical shape.

The free body diagram of the central mass is shown in **Figure 6** and at the displacement, *d*, the force balances of the central mass in the vertical axis yields:

$$m\ddot{d} + mg + \sin\alpha \int dF_{DEO} = 0, \qquad \text{Equation (4)}$$

where m is the mass of the central mass, $\ddot{d}$ is the vertical acceleration of the central mass, g is the gravitational acceleration and $\int dF_{DEO}$ is the total radial force exerted by the membrane on the central mass.

By assumption (**iii** & **iv**), the radial stress, σ_1, is assumed to be constant with respect to the cross-sectional area, and $\int dF_{DEO}$ in Equation (4) can be expressed as:

$$\int dF_{DEO} = \int_0^{2\pi} aT_2\sigma_1\, d\theta = 2\pi aT_2\sigma_1\,, \qquad \text{Equation (5)}$$

where θ is an angle that varies from 0 to 2π.

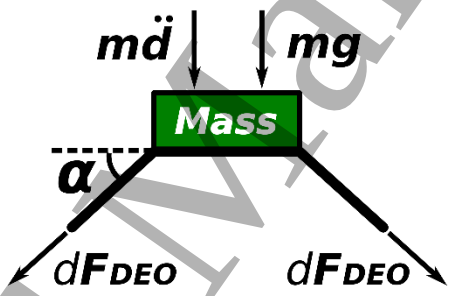

Figure 6. Free body diagram of the central mass on the DEO.

In order to take the viscoelasticity of the elastomer into account, we adopt the Bergstrom-Boyce rheological model [32] with two parallel units: spring 1 as a unit and spring 2 in series with a dashpot as the second unit, as depicted in **Figure 7**. The deformation of the membrane is described by the radial and the circumferential stretches, λ_1 and λ_2. For spring 1, its deformation is characterized by λ_1 and λ_2. However, for spring 2, its deformation is characterized by λ_1^e and λ_2^e due to the dashpot. Let ξ_1 and ξ_2 be the stretches of the dashpot and because the two units have the same net stretches, λ_1 and λ_2, the stretches for spring 2 can be written as:

$$\lambda_1^e = \frac{\lambda_1}{\xi_1}, \lambda_2^e = \frac{\lambda_2}{\xi_2}\,. \qquad \text{Equation (6)}$$

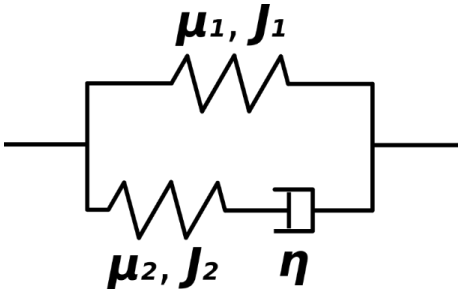

Figure 7. Two units rheological model representing the viscoelasticity of the elastomer. One unit consists of a spring and another unit consists of a spring in series with a dashpot.

To describe the radial stress as a function of the stretches of the membrane and the applied voltage, the Gent model was adopted in this work [33] and the viscoelasticity model was adopted from [34]. For an in-depth and complete description of the viscoelasticity model, please refer to [34]. The radial and circumferential stresses can be described as:

$$\sigma_1 = \frac{\mu_1\left(\lambda_1^2-\lambda_1^{-2}\lambda_2^{-2}\right)}{1-\left(\lambda_1^2+\lambda_2^2+\lambda_1^{-2}\lambda_2^{-2}-3\right)/J_1} + \frac{\mu_2\left(\lambda_1^{e2}-\lambda_1^{e-2}\lambda_2^{e-2}\right)}{1-\left(\lambda_1^{e2}+\lambda_2^{e2}+\lambda_1^{e-2}\lambda_2^{e-2}-3\right)/J_2} - \varepsilon_0\varepsilon_r E^2, \qquad \text{Equation (7)}$$

$$\sigma_2 = \frac{\mu_1\left(\lambda_2^2-\lambda_1^{-2}\lambda_2^{-2}\right)}{1-\left(\lambda_1^2+\lambda_2^2+\lambda_1^{-2}\lambda_2^{-2}-3\right)/J_1} + \frac{\mu_2\left(\lambda_2^{e2}-\lambda_1^{e-2}\lambda_2^{e-2}\right)}{1-\left(\lambda_1^{e2}+\lambda_2^{e2}+\lambda_1^{e-2}\lambda_2^{e-2}-3\right)/J_2} - \varepsilon_0\varepsilon_r E^2. \qquad \text{Equation (8)}$$

where μ_1 and μ_2 are the shear moduli of the two springs, J_1 and J_2 are constants of the limiting stretches of the two springs, ε_0 and ε_r are the absolute permittivity of vacuum and the relative permittivity of the dielectric elastomer respectively, E is the electric field applied across the membrane and is given as $E = V/T$, with voltage, V, and membrane thickness, T.

The first and second part on the right-hand side of Equations (7&8) represents the elastic stresses on spring 1 and spring 2 respectively, and the last part shows the voltage-induced Maxwell stress. It should be noted that the Gent hyperelastic model represents a nonlinear stress-strain relationship, which indicates the force-displacement relationship of the DEO will be nonlinear. The nonlinear 'sine' term in Equation (4) also adds effects on the nonlinearity of F_{DEO} in the vertical axis.

By modelling the dashpot as a Newtonian fluid [34], the rate of deformation of the dashpot in Equation (6) can be described as:

$$\frac{d\xi_1}{dt} = \frac{\xi_1}{3\eta}\left(\frac{\mu_2\left(\lambda_1^{e2}-\lambda_1^{e-2}\lambda_2^{e-2}\right)}{1-\left(\lambda_1^{e2}+\lambda_2^{e2}+\lambda_1^{e-2}\lambda_2^{e-2}-3\right)/J_2} - \frac{\mu_2\left(\lambda_2^{e2}-\lambda_1^{e-2}\lambda_2^{e-2}\right)/2}{1-\left(\lambda_1^{e2}+\lambda_2^{e2}+\lambda_1^{e-2}\lambda_2^{e-2}-3\right)/J_2}\right), \qquad \text{Equation (9)}$$

$$\frac{d\xi_2}{dt} = \frac{\xi_2}{3\eta}\left(\frac{\mu_2\left(\lambda_2^{e2}-\lambda_1^{e-2}\lambda_2^{e-2}\right)}{1-\left(\lambda_1^{e2}+\lambda_2^{e2}+\lambda_1^{e-2}\lambda_2^{e-2}-3\right)/J_2} - \frac{\mu_2\left(\lambda_1^{e2}-\lambda_1^{e-2}\lambda_2^{e-2}\right)/2}{1-\left(\lambda_1^{e2}+\lambda_2^{e2}+\lambda_1^{e-2}\lambda_2^{e-2}-3\right)/J_2}\right). \qquad \text{Equation (10)}$$

Note that based on assumption (**iv**), the circumferential deformation is unchanged during out-of-plane deformation, i.e. its value is changed only with pre-stretch. Hence in this simplified model, the circumferential stress, σ_2, does not need to be considered and the stretch of spring in circumferential axis remains constant: $\lambda_2^e = 1$. By substituting Equation (7) into (5) and solving the ordinary differential equations (4&9), the dynamic response of a DEO as function of excitation voltage can be estimated. In this work, these equations were solved numerically using MATLAB (MathWorks).

4. Experiment

4.1 Quasi-static force-displacement test experimental setup

A force-displacement test was performed to identify the quasi-static model parameters. The experimental setup is shown in **Figure 8**. The DEO frame was fixed to the testing rig and a linear rail (X-LSQ150B-E01, ZABER) deformed the centre of the DEO membrane out-of-plane at a low velocity of 0.05 mm/s to ensure negligible viscoelasticity. A constant voltage was generated by a high voltage amplifier (5HV23-BP1, Ultravolt) and was applied to the DEO during deformation to analyse the effect of electric field on the force-displacement relationship. The voltage amplitude was determined by $V = E\lambda_p^2/T_0$, where E = 50 V/μm. A load cell (NO.1004, TEDEA) was used to measure the reaction force of the DEO and a laser displacement sensor (LK-G152 and LKGD500, Keyence) was used to measure the deformation of the DEO membrane. All signals were collected by a DAQ device (National Instruments, BNC-2111) at a sampling frequency of 10,000 Hz and controlled by MATLAB (MathWorks).

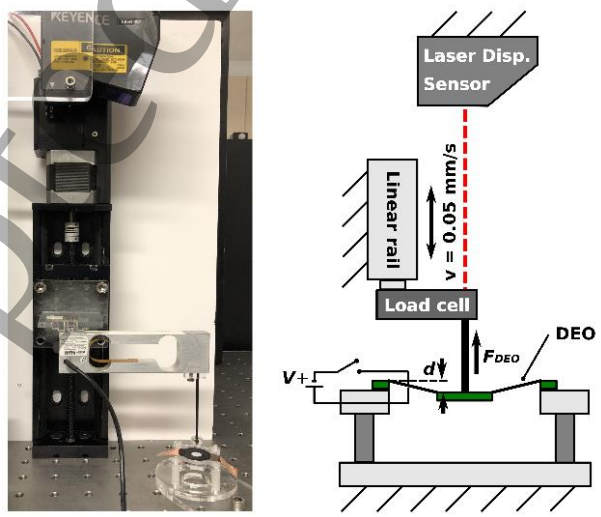

Figure 8. Photo and schematic diagram of the experimental setup for quasi-static force-displacement measurement.

4.2 Dynamic test experimental setup

A frequency sweep test was performed to investigate the dynamic performance of the DEO at different excitation frequencies and to identify the dynamic model parameters. The experimental setup is shown in **Figure 9**. The DEO frame was fixed to the testing rig, while leaving the central mass to move freely. A varying-frequency sinusoidal voltage signal was generated by MATLAB and applied to the DEO via a high voltage amplifier. A laser displacement sensor measured the out-of-plane deformation of the DEO at a sampling frequency of 40,000 Hz. The excitation frequency was swept forward from 0 to 300 Hz (300 to 0 Hz for a backward sweep) at the rate of 1 Hz/s, generated by MATLAB using 'chirp' function (the DC biasing voltage, V_{DC} , and the AC voltage amplitude, V_{AC}, are determined by $V_{DC} = E_{DC}\lambda_p^2/T_0$, $V_{AC} = E_{AC}\lambda_p^2/T_0$ and a value of E_{DC}=E_{AC}=25 V/μm was used in the test). An example waveform of this frequency sweep is shown in **Figure 10**. As the frequency will vary continuously during this test, the system will not reach its steady state. To account for this, a second test, where the frequency was varied in discrete steps, was also adopted. These steps are given by the voltage signal : $V(t) = V_{DC} + V_{AC} \sin 2\pi\Omega t$ with the frequency Ω stepped up from 1 to 300 Hz then down to 1 Hz by steps of 0.1 Hz, 20 cycles of excitation signals were repeated at each frequency to ensure the DEO reached a steady-state response. An example waveform of this frequency step is given in **Figure 11**.

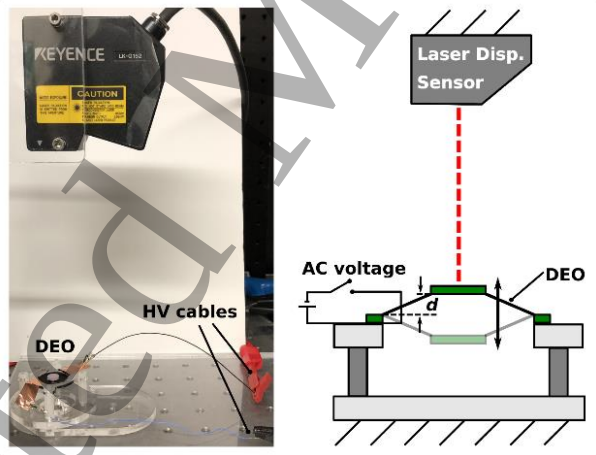

Figure 9. Photo and schematic diagram of the experimental setup for active dynamic tests.

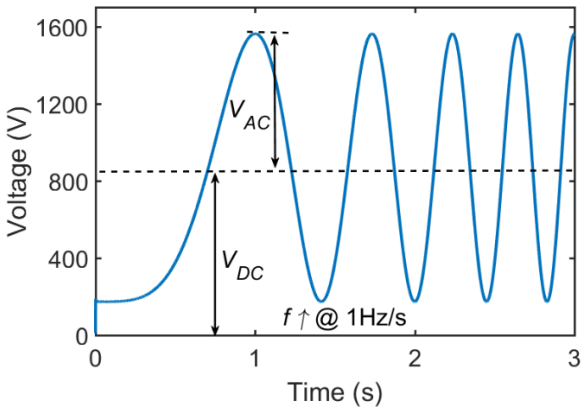

Figure 10. Example of a sinusoidal frequency sweep. The wave consists of two parts: a DC biasing voltage V_{DC} and an AC voltage with the amplitude of V_{AC}. The frequency is increased continuously from 1 to 300 Hz at a rate of 1 Hz/s.

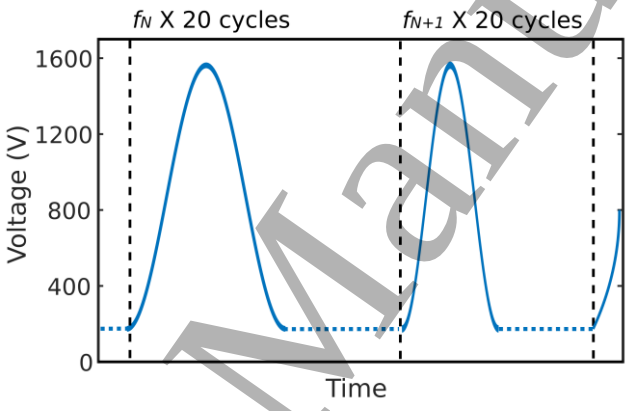

Figure 11. Example of a sinusoidal frequency step wave. The frequency is stepped from 1 to 300 Hz with the step of 0.1 Hz. 20 cycles are repeated at each frequency.

5. Experimental results

5.1 Quasi-static force-displacement results

To analyse the quasi-static response of the DEO and identify the parameters for the Gent model, the DEO was deformed out-of-plane at a very slow rate (0.05 mm/s) to reduce the viscoelastic effects. The model parameters were determined by fitting to the experimental results using a least-mean-squared algorithm in MATLAB (following [19]). The identified Gent model parameters are: μ_1 = 433.6 kPa, J_1 = 20.22. A relative permittivity ε_r = 2.8 was adopted in this model for Elastosil elastomer, as measured by the manufacturer [35]. As can be seen in **Figure 12** (**a-c**), the model agrees very well with the experiments with different pre-stretches. Note that the force-displacement relationship is nonlinear with a stiffening effect, which suggested that its dynamic response will also be nonlinear.

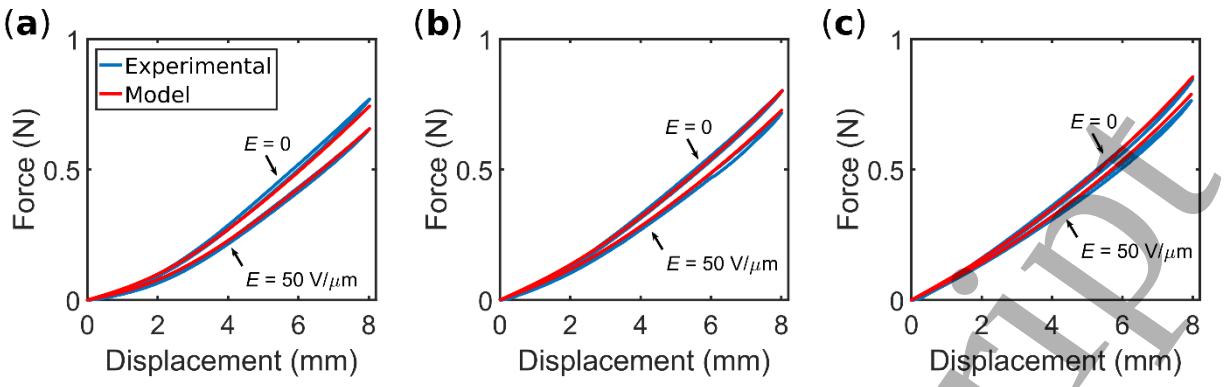

Figure 12. Model validation: quasi-static force-displacement relationship with and without actuation voltage. (**a**) λ_p = 1.1 × 1.1; (**b**) λ_p = 1.2 × 1.2; (**c**) λ_p = 1.3 × 1.3.

5.2 Active dynamic test results

The model parameters related to the viscoelasticity of the elastomer were identified by a forward frequency sweep test. The DEO was excited by a varying frequency voltage waveform from 0 to 300 Hz with the sweep rate of 1 Hz/s. The dynamic model parameters were also tuned by a best-fit principle and the values obtained are μ_2 = 400 kPa, J_2 = 20, η= 2 kPa·s. **Figure 13** (**a**-**b**) shows the experimental results of forward and backward frequency sweep and the model prediction is shown in **Figure 13** (**c**-**d**). The nonlinearity of this DEO can be clearly observed from the frequency sweep experimental results and model predictions. The amplitude of the DEO was very close to zero at low frequencies, and large amplitudes only occur at the resonance, where the amplitude increases with the increasing frequency before dropping sharply after the resonant frequency in the forward frequency sweep. On the contrary, in the backward frequency sweep, as the frequency decreases, the amplitude jumps suddenly from an extremely low value to its peak and then reduces as the frequency decreases. Also note the peak amplitude in the backward sweep is much lower than that in the forward sweep (13.5 mm at Ω = 275 Hz for forward sweep and 3.8 mm at 219 Hz for backward sweep). Note that the two large peaks shown in **Figure 13** (**a**) belong to the first resonant mode where the deformation of the membrane is axially symmetrical and the largest deformation is in the centre, as demonstrated in the high-speed photos in **Figure 14** (**a**). Further increasing the frequency causes the DEO to vibrate at its second resonant mode, as is shown in **Figure 14** (**b**) (high speed video available in the supplementary material). The second resonant mode cannot be characterized using this numerical model (1 DOF assumption was made in this model). This extremely complex dynamic behaviour is out the scope of this work and requires further investigation in future.

It is worth noticing that the maximum stroke of the DEO in the forward frequency was measured at 13.5 mm, which is 67.5 % relative to the membrane diameter. By contrast, in previous studies, the

demonstrated resonant stroke was much smaller relative to the membrane diameter, for example, ~ 4 % stroke in [12] and ~ 7 % in [13] using VHB material and 30 % in [16] using silicone elastomer. It should be noted that the high out-of-plane deformation of the silicone can potentially lead to mechanical rupture. By using the model developed in this work, the maximum radial stretch during deformation is estimated at 1.85, which is significantly lower than the elongation at break value of 4.5 reported by the manufacturer [35]. It is worth noting that in this model, simplification was made such that the stretch is homogeneous along the radial axis, however, in reality the radial stretch closes the boundary with the mass can be much higher than the average value [36], thus resulting in a mechanical rupture in that local region.

To illustrate the function of the central mass in this DEO design, a comparison was made by running a similar forward frequency sweep on a DEO sample with no central mass attached to the membrane. One significant difference between DEOs with and without a central mass is the resonant frequency. Without the mass attached, the excitation frequency where the highest peak occurs was found at ~ 750 Hz, while the one with the mass has its peak at 275 Hz. The experimental result of the no added mass DEO can be found in **Figure S1** (**a**) in the supplementary material. Another difference is in the deformation shape, as the DEOs with mass attached in the centre have an approximated conical shape, while the one without mass is closer to a dome shape, as illustrated in **Figure S1** (**b**).

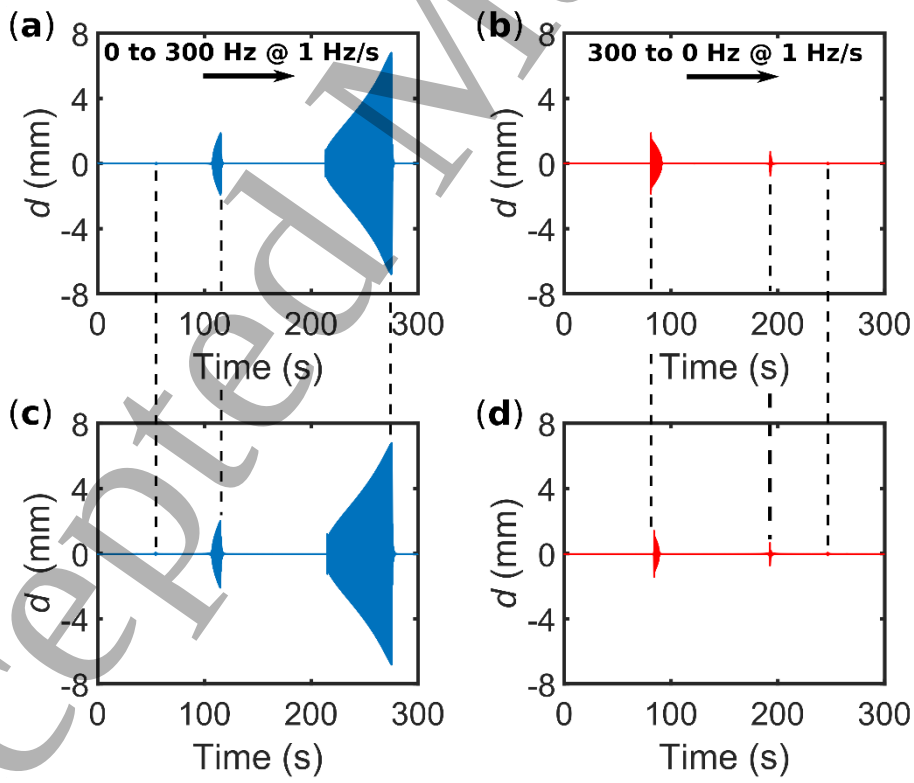

Figure 13. Model validation: frequency sweep test. (**a**) measured displacement of the DEO in a forward sweep and (**b**) a backward sweep. (**c**) modelled displacement of the DEO in a forward sweep and (**d**) a backward sweep.

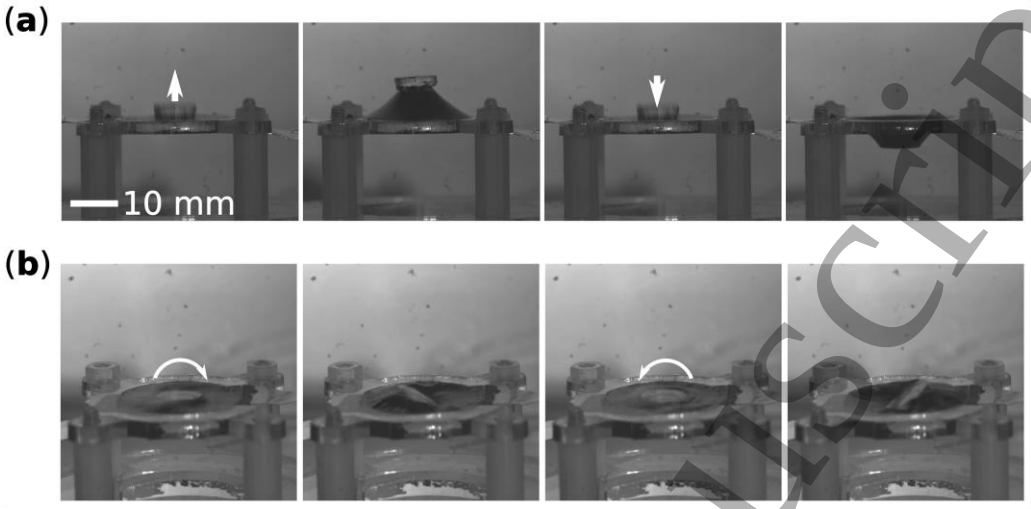

Figure 14. High-speed video frames of the DEO oscillating out-of-plane in the (**a**) first resonate mode and (**b**) second resonate mode.

5.3 Frequency domain analysis

Figure 15 shows the measured time domain data of the DEO in a frequency step experiment where the frequency was increased from 1 to 300 Hz at a step of 0.1 Hz. By using discrete Fourier transform (DFT), **Figure 16** (**a**-**b**) plots the fundamental response frequency ω (which is defined as the frequency of the component with the largest amplitude in a DFT) and amplitude against the excitation frequency Ω. The last 10 cycles at each frequency (allowing 10 cycles for the DEO to reach a steady-state) in a frequency step test was used in the DFTs. It can be seen clearly from **Figure 16** (**a**), that for this proposed DEO, the fundamental harmonics do not always match the excitation frequency, and a subharmonic of 1/2 and super-harmonics at 2, 3, 4 can be observed. This is due to the nonlinearity that is inherent in such a system. In **Figure 16** (**b**), at the low frequencies (e.g. < 50 Hz), the amplitude is close to zero, a small peak of 0.15 mm can be found at 54 Hz and two significantly larger amplitude peaks occur above 100 Hz. The highest resonant peak is found at 275 Hz with an amplitude of 13.5 mm and the second highest resonant peak is at 118 Hz with an amplitude of 5 mm. It can be noted that the two resonant peaks are distorted to the right and completely different behaviors are obtained for stepping down the excitation frequencies. For example, as the excitation frequency Ω increases from 200 to 280 Hz, the amplitude gradually increases until it reaches a point at Ω = 275 Hz. If Ω is increased beyond this point, a limit point is approached, and the response jumps down to a lower stable branch. However, when decreasing Ω from above the resonance point, the amplitude follows the lower branch until 218.8

Hz and suddenly jumps up to the upper stable branch, as illustrated in **Figure 16** (**b**). The region between the two jump points is a region with multiple stable solutions, which is characteristic of a forced response of a nonlinear dynamic system [37] [38].

Figure 17 shows the detailed time series of the input (actuation voltage) and output (displacement) signals and the frequency spectrum of the five points a-e in **Figure 15**. Only point d exhibits $\omega = \Omega$ (**Figure 17** (**d**)), i.e. the fundamental response frequency is equal to the excitation frequency, while for the other four points a, b, c, and e, the fundamental frequency of the response is different to the excitation frequency, as indicated in the frequency spectra. For point e where the amplitude has the highest peak (**Figure 17** (**e**)), the fundamental response period is twice that of the excitation period and in the frequency spectrum the highest peak is a 1/2 Ω subharmonic. In the other three cases, different integer super-harmonics are observed in **Figure 17** (**a-c**).

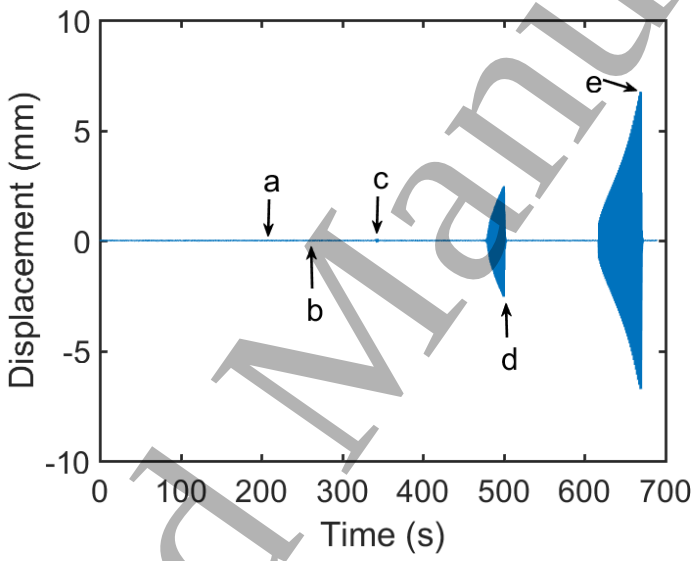

Figure 15. Frequency step response experimental results. Five points are marked from a to e representing five distinguishable types of responses.

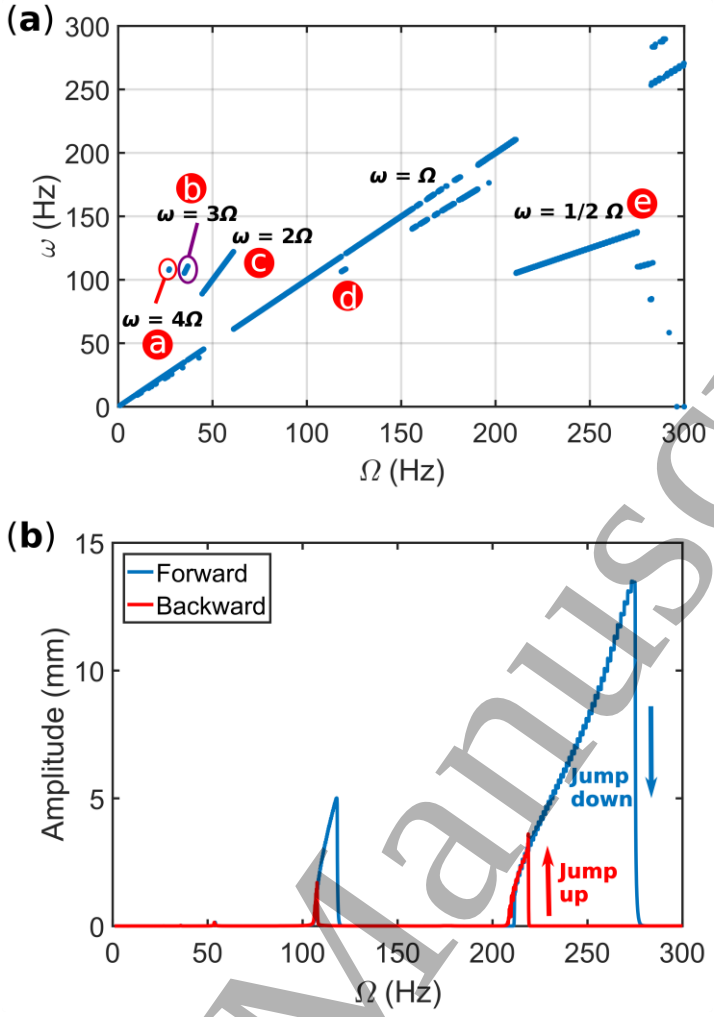

Figure 16. Frequency step results in frequency domain. (**a**) Fundamental response frequency against excitation frequency, subharmonics, harmonic and super-harmonic responses can be observed. (**b**) Amplitude against excitation frequency. Jump down and jump up can be noticed in the forward and backward sweep respectively.

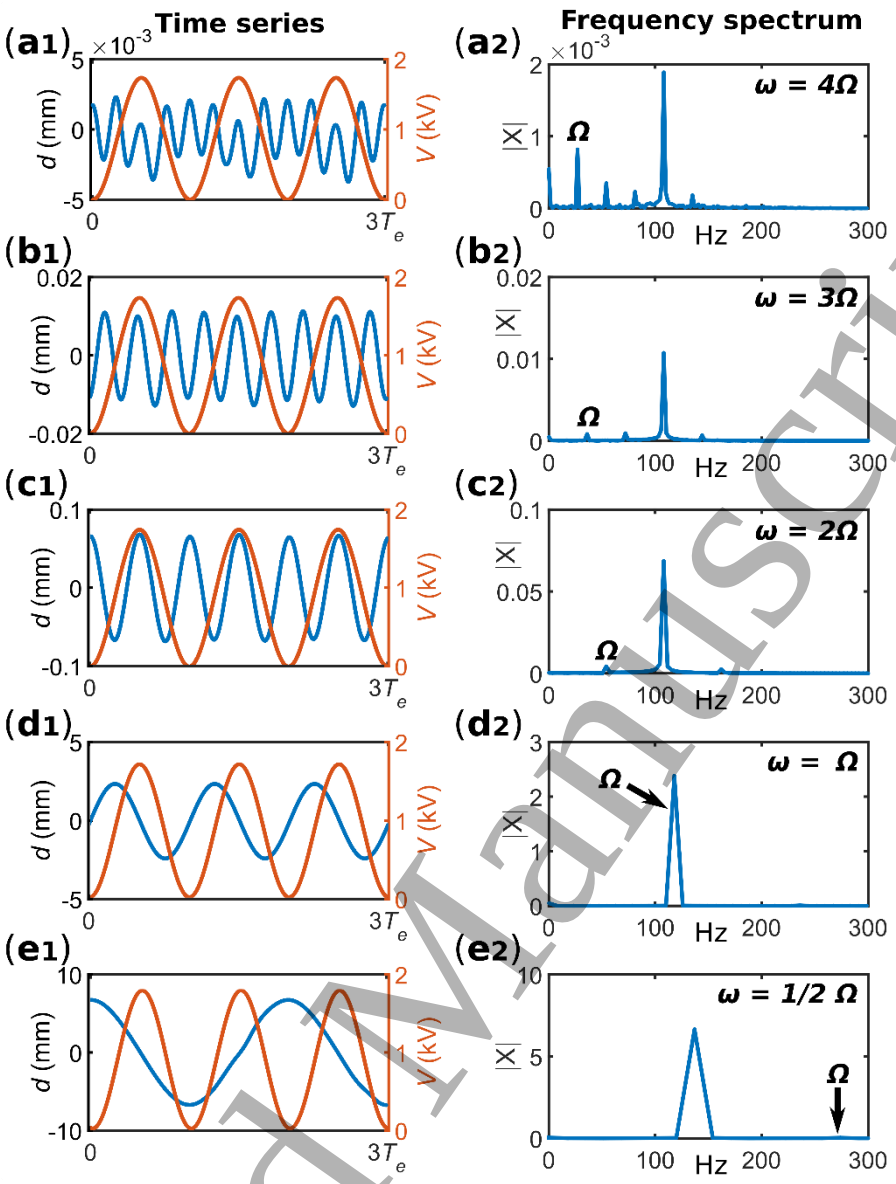

Figure 17. Five different frequency responses of a circular DEO. The time series on the left and the frequency spectra on the right, where d is the displacement of the oscillator, V is the actuation voltage and $|X|$ is the absolute value of DFT amplitude. (**a**) $\omega = 4\,\Omega$, Ω = 27 Hz, (**b**) $\omega = 3\,\Omega$, Ω = 36 Hz, (**c**) $\omega = 2\,\Omega$, Ω = 60 Hz, (**d**) $\omega = \Omega$, Ω = 118 Hz, (**e**) $\omega = 1/2\,\Omega$, Ω = 275 Hz.

6. Further studies on the DEO dynamics

In this section, the effects of varying the DEO parameters on the dynamic responses are investigated. First, the mechanical parameters such as the pre-stretch ratios and the weight of the mass are considered. Second, the effects of the electrical signal (i.e. the AC and DC components) are analysed.

6.1 Effects of the central mass and pre-stretch ratios

This sub-section compares the effects of the added mass and pre-stretch on the dynamic performance of the DEO. One parameter was fixed constant while varying the other. **Figure 18** shows the experimental and simulated DEO frequency response with different masses (0.1, 0.12 and 0.2 g). Detailed values of the resonant amplitudes and the resonant frequencies are listed in **Table S2** in the supplementary material. The pre-stretch ratio was fixed at λ_p = 1.2 × 1.2 and the same sine wave frequency step test described in Section 4.2 with $E_{DC} = E_{AC}$ = 25 V/μm was adopted here. It can be noted that as the mass increases, the resonant amplitude increases, and the resonant frequency reduces. The maximum amplitude of 15.9 mm was measured with m = 0.2 g, which is equivalent to ~ 80 % relative to the membrane diameter. Also note that the model was able to predict the nonlinear dynamic response of the DEOs with different added masses accurately.

In the second test, the performance of DEOs with different pre-stretch ratios (λ_p = 1.1 × 1.1, λ_p = 1.2 × 1.2, λ_p = 1.3 × 1.3) were compared and the results are shown in **Figure 19**. Detailed values of the measured and modelled resonant amplitudes and the resonant frequencies can be found in **Table S3** in Supplementary. The central mass was fixed at m = 0.1 g, and the electric field was $E_{DC} = E_{AC}$ = 25 V/μm. It can be noted that, as the pre-stretch ratio increases, the resonant frequency increases as the membrane becomes stiffer (**Figure 12**); however, there is no clear effect on the resonant amplitude. Note that the model underpredicted amplitude of the first peak (near 100 Hz in **Figure 19** (**a**)) in the case of λ_p = 1.1 × 1.1 and the second peak (near 295 Hz in **Figure 19** (**c**)) in the case of λ_p = 1.3 × 1.3. Despite this, the estimated resonant frequency (295.5 Hz) is very close to the measured resonant frequency (295.3 Hz). The difference between model prediction and experimental results could be due to a slight mismatch in the force-displacement relationship with λ_p = 1.1 × 1.1 and λ_p = 1.3 × 1.3, since the model parameters were identified based on experimental results with λ_p = 1.2 × 1.2.

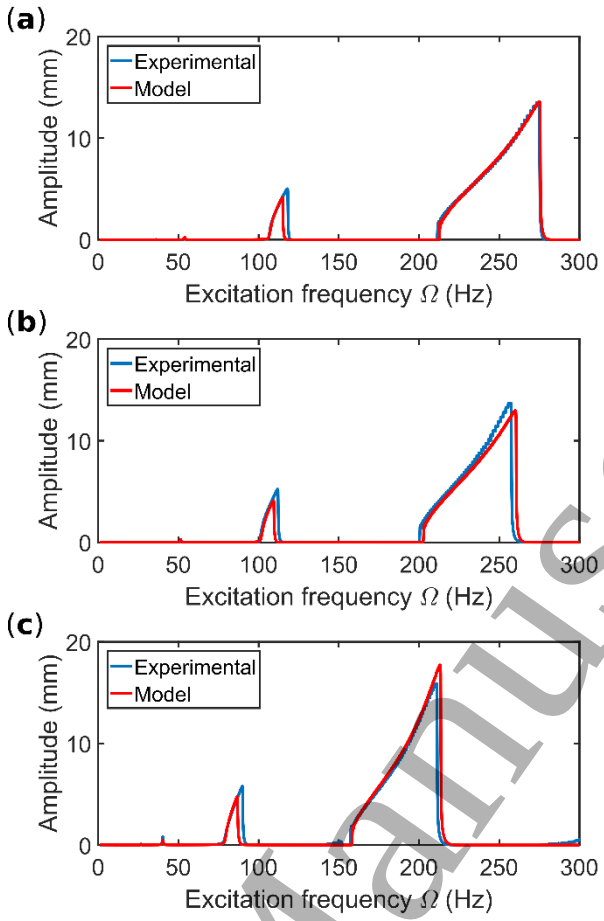

Figure 18. Oscillation amplitude against excitation frequency of the DEOs with different added mass. (**a**) m = 0.1 g; (**b**) m = 0.12 g; (**c**) m = 0.2 g.

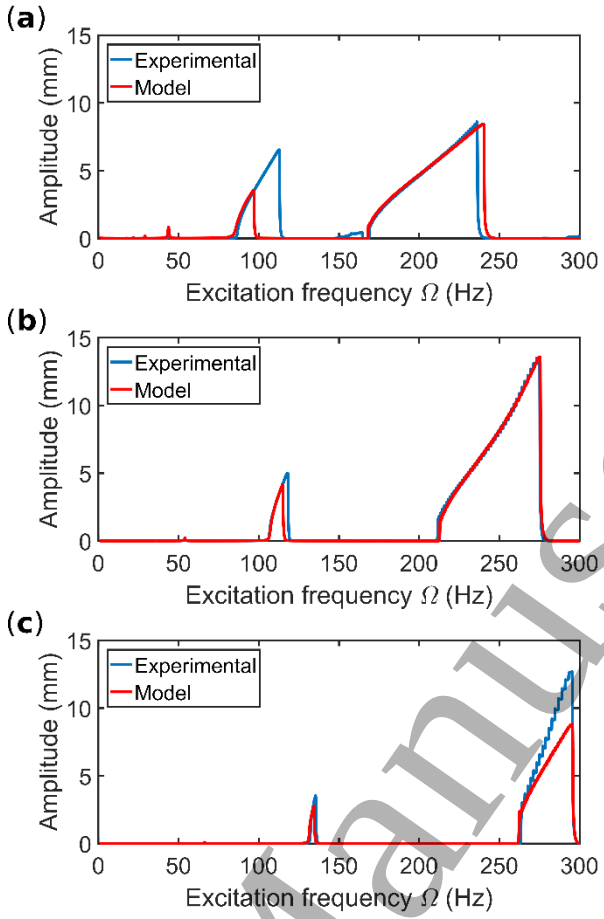

Figure 19. Oscillation amplitude against excitation frequency of the DEOs with different pre-stretch ratios. (**a**) λ_p = 1.1 × 1.1; (**b**) λ_p = 1.2 × 1.2; (**c**) λ_p = 1.3 × 1.3.

6.2 Effects of the actuation signal

In this sub-section, we investigate the effect of the actuation signal on the dynamics of the DEOs. Here the pre-stretch ratio and the central mass were fixed at λ_p = 1.2 × 1.2 and m = 0.1 g. An example of the composition of a sine frequency sweep waveform can be found in **Figure 10**. The electric field parameters: AC electric field amplitude, E_{AC}, and DC biasing electric field, E_{DC}, were varied in this section with the rule of $E_{AC} \leq E_{DC}$ (voltage must be greater than zero).

First, E_{DC} was varied from 15 to 25 V/μm while fixing E_{AC} at 15 V/μm and the result is shown in **Figure 20**. When the E_{DC} = 15 V/μm, a very low resonant amplitude was reached (~ 0.3 mm) and, as E_{DC} increased by 5 V/μm, the amplitude increased dramatically to a value of 6.7 mm and, as E_{DC} increased further, the amplitude continued to increase, and the high amplitude can be obtained at a wider range of excitation frequencies. This is possibly due to the fact that, as the DC biasing electric field increases, the induced Maxwell stress (proportional to E^2) causes a greater reduction in the total stress, causing the DEO membrane to be 'softer' and an out-of-plane resonance can be triggered more easily.

In the second test, the DC biasing electric field, E_{DC}, was fixed at 25 V/μm and E_{AC} increased from 10 to 25 V/μm. The experimental results are shown in **Figure 21** and, as expected, both the resonant frequency and the amplitude increase with the increasing E_{AC} and the high amplitude region becomes broader. The results indicate that the resonant frequency and amplitudes of the DEOs can be easily tuned by the electrical signal (i.e. varying E_{AC} and E_{DC}) to meet applications where specific resonance response/amplitude is desired.

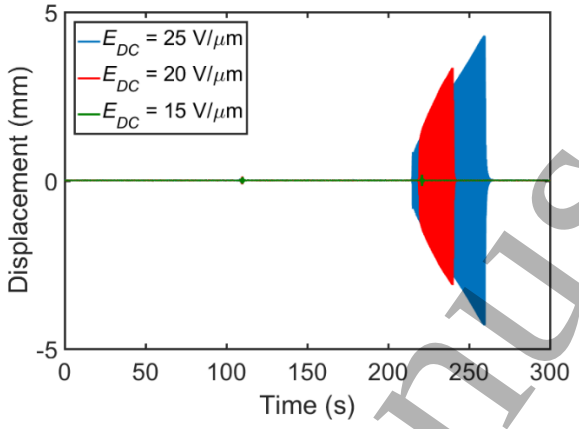

Figure 20. Comparison of the displacement of the DEO in a frequency sweep with different biasing DC voltage amplitudes. E_{AC} = 15 V/μm in all cases.

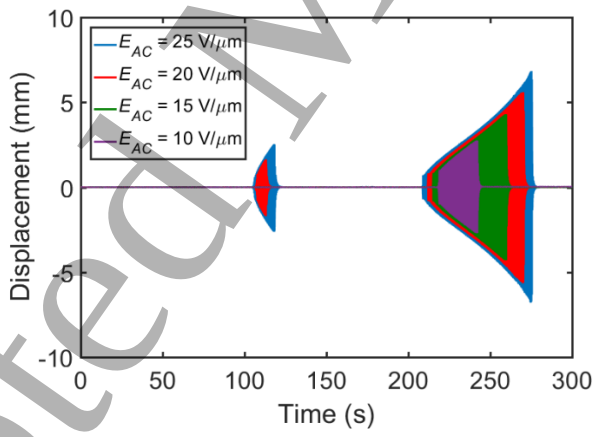

Figure 21. Comparison of the displacement of the DEO in a frequency sweep with different AC voltage amplitudes. E_{DC} = 25 V/μm in all cases.

7. Conclusion

To summarize, in this work we presented a circular planar DEO which exhibits highly nonlinear phenomena. First, a custom carbon grease was developed to eliminate the swelling issue in silicone elastomers with commercial carbon greases. A simplified mathematical model was proposed to analyze the complex nonlinearity of the DEO, and good agreement was found with both quasi-static force-

displacement responses and the experimental results showing dynamic responses. Hence, this model can support the adoption of this silicone membrane-based DEO in a variety of new applications. The hyper-elasticity of the elastomer and the complex three-dimensional deformation of this oscillator leads to highly nonlinear behavior. This oscillator was found to have multiple resonant peaks and the responses at these peaks were shown to contain strong subharmonic, harmonics and super-harmonic responses. By comparing the DEOs with different pre-stretch ratios, central mass weights and excitation voltage signals (i.e. AC and DC amplitudes), we showed that (**i**) resonance of the DEOs with higher pre-stretch ratios will occur at higher frequencies; (**ii**) increasing the weight of the central mass will increase the resonant amplitude but reduce the resonant frequency; (**iii**) adjusting the DC biasing electric field can controllably trigger significantly larger (~ 20 times) out-of-plane oscillations and increasing the AC electric field can increase the resonant amplitudes and the corresponding resonant frequencies. This low-profile planar oscillator has advantages over other oscillation actuators in its highly tunable oscillation amplitudes and frequencies by simply adjusting either the physical parameters or the actuation voltage signals. This oscillator demonstrates a maximum out-of-plane stroke of about 80 % of the DEO membrane diameter at its resonance. Such large stroke output and highly tunable resonance make this DEO a promising candidate for applications such as active vibration absorption, soft pumps and robotic locomotion.

Acknowledgement

C.C. acknowledges the support from the EPSRC Centre for Doctoral Training in Future Autonomous and Robotic Systems (FARSCOPE) at the Bristol Robotics Laboratory. A. C. appreciates the support by EPSRC grant EP/P025846/1.

References

[1] R. Pelrine, R. Kornbluh, Q. Pei and J. Jose Joseph, "High-Speed Electrically Actuated Elastomers with Strain Greater Than 100%," *Science*, pp. 836-839, 2000.

[2] C. Jenkins, "Nonlinear dynamic response of membranes: State of the art-Update," *Applied Mechanics Reviews*, vol. 49, no. 10S, pp. S41-S48, 1996.

[3] C. Jenkins and U. Korde, "Membrane vibration experiments: an historical review and recent results," *Journal of Sound and Vibration*, vol. 295, pp. 602-613, 2006.

[4] P. Gonçalves, R. Soares and D. Pamplona, "Nonlinear vibrations of a radially stretched circular hyperelastic membrane," *Journal of Sound and Vibration*, vol. 327, no. 1-2, pp. 231-248, 2009.

[5] J. Fox and N. Goulbourne, "Electric field-induced surface transformations and experimental dynamic characteristics of dielectric elastomer membranes," *Journal of the Mechanics and Physics of Solids*, vol. 57, no. 8, pp. 1417-1435, 2009.

[6] J. Fox and N. Goulbourne, "On the dynamic electromechanical loading of dielectric elastomer membranes," *Journal of the Mechanics and Physics of Solids*, vol. 56, no. 8, pp. 2669-2686, 2008.

[7] J. Zhu, S. Cai and Z. Suo, "Nonlinear oscillation of a dielectric elastomer balloon," *Polymer International*, vol. 59, no. 3, pp. 378-383, 2010.

[8] J. Zhu, S. Cai and Z. Suo, "Resonant behavior of a membrane of a dielectric elastomer," *International Journal of Solids and Structures*, vol. 47, no. 24, pp. 3254-3262, 2010.

[9] C. Cao, X. Gao and A. T. Conn, "A compliantly coupled dielectric elastomer actuator using magnetic repulsion," *Applied Physics Letters*, vol. 114, no. 1, p. 011904, 2019.

[10] C. Cao, S. Burgess and A. T. Conn, "Towards a dielectric elastomer resonator driven flapping wing micro air vehicle," *Frontiers in Robotics and AI*, vol. 5, p. 137, 2018.

[11] C. Keplinger, J. Y. Sun, C. C. Foo, P. Rothemund, G. M. Whitesides and Z. Suo, "Stretchable, transparent, ionic conductors," *Science*, vol. 341, no. 6149, pp. 984-987, 2013.

[12] U. Chakravarty, "On the resonance frequencies of a membrane of a dielectric elastomer," *Mechanics Research Communications*, vol. 55, pp. 72-76, 2014.

[13] C. Tang, B. Li, W. Sun, Z. Li and H. Chen, "Identification and characterization of the out-of-plane resonance in a dielectric elastomer to drive an agile robotic cube," *Journal of Applied Physics*, p. 165104, 2017.

[14] C. Tang, B. Li, H. Fang, Z. Li and H. Chen, "A speedy, amphibian, robotic cube: Resonance actuation by a dielectric elastomer," *Sensors and Actuators A: Physical*, pp. 1-7, 2018.

[15] Y. Li, I. Oh, J. Chen and Y. Hu, "A new design of dielectric elastomer membrane resonator with tunable resonant frequencies and mode shapes," *Smart Materials and Structures*, vol. 27, no. 6, p. 065029, 2018.

[16] X. Gao, C. Cao, J. Guo and A. T. Conn, "Elastic electroadhesion with rapid release by integrated resonant vibration," *Advanced Materials Technologies,* vol. 4, no. 1, p. 1800378, 2019.

[17] R. Palakodeti and M. Kessler, "Influence of frequency and prestrain on the mechanical efficiency of dielectric electroactive polymer actuators," *Materials Letters,* p. 3437–3440, 2006.

[18] G. Kofod, "The static actuation of dielectric elastomer actuators: How does pre-stretch improve actuation?," *Journal of Physics D: Applied Physics,* p. 215405, 2008.

[19] M. Hodgins, G. Rizzello, D. Naso, A. York and S. Seelecke, "An electro-mechanically coupled model for the dynamic behavior of a dielectric electro-active polymer actuator," *Smart Materials and Structures,* p. 104006, 2014.

[20] S. Hau, D. Bruch, G. Rizzello, P. Motzki and S. Seelecke, "Silicone based dielectric elastomer strip actuators coupled with nonlinear biasing elements for large actuation strains," *Smart Materials and Structures,* vol. 27, no. 7, p. p.074003, 2018.

[21] S. Hau, G. Rizzello, M. Hodgins, A. York and S. Seelecke, "Design and control of a high-speed positioning system based on dielectric elastomer membrane actuators," *IEEE/ASME Transactions on Mechatronics,* vol. 22, no. 3, pp. 1259-1267, 2017.

[22] M. Hodgins and S. Seelecke, "Systematic experimental study of pure shear type dielectric elastomer membranes with different electrode and film thicknesses," *Smart Materials and Structures,* vol. 25, no. 9, p. p.95001, 2016.

[23] D. T. Kuhnel, J. M. Rossiter and C. F. Faul, "Laser-Scribed Graphene Oxide Electrodes for Soft Electroactive Devices," *Advanced Materials Technologies,* p. 1800232, 2018.

[24] S. Rosset and H. Shea, "Flexible and stretchable electrodes for dielectric elastomer actuators," *Applied Physics A: Materials Science and Processing*, vol. 110, no. 2, pp. 281-307, 2013.

[25] R. Pelrine, R. Kornbluh, J. Joseph, R. Heydt, Q. Pei and S. Chiba, "High-field deformation of elastomeric dielectrics for actuators," *Materials Science and Engineering C*, vol. 11, no. 2, pp. 89-100, 2000.

[26] B. O'Brien, J. Thode, I. Anderson, E. Calius, E. Haemmerle and S. Xie, "Integrated extension sensor based on resistance and voltage measurement for a dielectric elastomer," in *Electroactive Polymer Actuators and Devices (EAPAD) 2007*, San Diego, 2007.

[27] L. M. Diamante and T. Lan, "Absolute viscosities of vegetable oils at different temperatures and shear rate range of 64.5 to 4835 s− 1," *Journal of food processing*, 2014.

[28] J. Germann, B. Schubert and D. Floreano, "Stretchable electroadhesion for soft robots," in *IEEE/RSJ International Conference on Intelligent Robots and Systems (IROS 2014)*, 2014.

[29] K. M. Digumarti, C. Cao, J. Guo, A. T. Conn and J. Rossiter, "Multi-directional crawling robot with soft actuators and electroadhesive grippers," in *2018 IEEE International Conference on Soft Robotics (RoboSoft)*, 2018.

[30] R. Huang and Z. Suo, "Electromechanical phase transition in dielectric elastomers," *Proceedings of the Royal Society A: Mathematical, Physical and Engineering Sciences*, vol. 468, no. 2140, pp. 1014-1040, 2011.

[31] F. Carpi, I. Anderson, S. Bauer, G. Frediani, G. Gallone, M. Gei, C. Graaf, C. Jean-Mistral, W. Kaal, G. Kofod and M. Kollosche, "Standards for dielectric elastomer transducers," *Smart Materials and Structures*, vol. 24, no. 10, p. 105025, 2015.

[32] J. Bergstrom and M. Boyce, "Constitutive Modeling of the Large Stain Time- Dependant Behaviour of elastomer," *Journal of Mechanics and Physics of Solids*, vol. 46, no. 5, pp. 931-954, 1998.

[33] A. N. Gent, "A New Constitutive Relation for Rubber," *Rubber Chemistry and Technology*, vol. 69, no. 1, pp. 59-61, 1996.

[34] C. C. Foo, S. Cai, S. J. Adrian Koh, S. Bauer and Z. Suo, "Model of dissipative dielectric elastomers," *Journal of Applied Physics,* vol. 111, no. 3, p. 034102, 2012.

[35] W. C. AG, "ELASTOSIL® FILM Electro-active Polymers (EAP) with Silicone Film," Wacker Chemie AG, [Online]. Available: https://www.wacker.com/cms/media/publications/downloads/7091_EN.pdf. [Accessed 20 1 2019].

[36] C. Cao and A. Conn, "Performance Optimization of a Conical Dielectric Elastomer Actuator," *Actuators,* vol. 7, p. 32, 2018.

[37] D. Wagg and S. Neild, Nonlinear Vibration with Control, Springer-Verlag, 2009.

[38] H. Hayfeh and T. Mook, Nonlinear oscillations, John Wiley & Sons, 2008.

[39] T. He, X. Zhao and Z. Suo, "Dielectric elastomer membranes undergoing inhomogeneous deformation," *Journal of Applied Physics,* vol. 106, no. 8, p. 083522, 2009.